JOURNAL OF MATERIALS SCIENCE 29 (1994) 203–212

# Single-fibre polymer composites

## Part II *Residual stresses and their effects in high-modulus polyethylene fibre composites*

D. T. GRUBB, ZONG-FU LI
*Department of Materials Science and Engineering, Cornell University, Ithaca, NY 14853, USA*

Raman spectroscopy of high-modulus polyethylene (PE) fibres embedded in epoxy resin shows that the axial compressive residual stress is constant at 0.3 GPa for curing conditions where the matrix shrinkage is larger than 0.2%. Optical microscopy shows that the fibre fails by forming kink bands at this strain. The local stress concentration around the kink bands then causes interfacial debonding. The axial strain in a fibre varied widely at the kink bands but no significant difference was found between the axial strain at a kink band and at a nearby position on the undamaged fibre. The PE fibres have a very small thermal coefficient of expansion (TCE) in the axial direction and an unusually large TCE in the radial direction, larger than that of the epoxy matrix. On cooling the composite after curing, a normal tensile stress develops at the interface between the fibre and epoxy, and in PE fibres without surface treatment this causes debonding of the interface. PE fibres with ammonia plasma surface treatment do not debond on cooling, but the interface is still weaker than that of other reinforcing fibre composites. One reason for this is the large radial TCE of these fibres. When the fibre is pulled through the matrix after interfacial debonding, the axial stress distribution shows that interfacial friction is established. The interfacial normal stress must change to a compressive stress during pull-out; the cross-section of the fibre is irregular. The normal stress and frictional coefficient can be obtained from the axial stress distribution. It is found that plasma-treated fibres have a much higher normal stress and frictional coefficient than untreated fibres. The load–displacement curves in single-fibre pull-out tests also show the differences in friction.

## 1. Introduction

The interfacial shear strength (IFSS) of a fibre-reinforced polymer composite is one of the key parameters in determining its mechanical properties. In general, a strong interface is required for a fibre composite to be an acceptable product. Much research has been focused on fibre surface treatments designed to achieve a strong interface, but the IFSS does not depend only on the fibre surface. For example, the IFSS for a graphite fibre can be over 100 MPa, whereas that for a Kevlar fibre never exceeds 100 MPa no matter what surface modification is applied. It appears that each fibre type has its own upper limit to IFSS. Intrinsic limiting factors may be due to the fibre internal structure and morphology and the resulting mechanical and thermal properties. High-modulus polymer fibres (such as aramids) and high-modulus polyethylene (PE) fibres consist of fibrils which have low interfibrillar bonding strength.

If the true IFSS exceeds the internal shear strength of the fibre, then the composite will fail under load when fibrils at the fibre surface separate from the rest of the fibre. Kalantar and Drzal [1] examined the interfacial failure mechanism for a Kevlar fibre in epoxy resin using transmission electron microscopy. They found that the fibre fibrillates near the interface due to the low cohesive strength of fibrils. This limits IFSS in tests which detect failure at or near the fibre surface. Other factors such as a large Poisson's ratio and low specific surface area due to large fibre diameter and low surface roughness will also weaken the interface.

Another important factor affecting IFSS and composite strength is the residual stress on the fibre, which has axial and radial components. The residual stress is caused by matrix curing shrinkage and the mismatch in TCE between fibre and matrix. During the preparation of composites, matrix curing or moulding shrinkage will lead to significant axial compressive stress along the fibres Axial compressive stress will also develop in the fibres on cooling the matrix to room temperature from its curing temperature or from the moulding temperature, due to the large difference in TCE between fibre and matrix. This is especially significant in the case of many high-modulus polymer fibres embedded in polymeric resins. Table I shows the TCE in fibre radial and axial directions for different fibres, their composite interfacial shear strength and the fibre compressive failure strain in matrix. Carbon, Kevlar and high-modulus

0022–2461 

TABLE I Axial and radial thermal expansion coefficients of Kevlar, carbon, and polyethylene fibres, their composite interfacial shear strength and compressive failure strains in the matrix, $\varepsilon_c$

| Property | Carbon | Kevlar | Polyethylene |
|---|---|---|---|
| TCE ($10^{-6}\,°C^{-1}$) [5–7] | | | |
| Axial | − 1.0 | − 5.7 | − 5.1 |
| Radial | 17 | 66 | 130 |
| IFSS (MPa) [8–10] | | | |
| Average, $\tau_a$ | 40–60 | 30–40 | 14 |
| Maximum, $\tau_s$ | 150 | 63 | 28 |
| $\varepsilon_c$ (%) [11, 12] | 0.5–1 | 0.25 | 0.2[a] |

[a] From this study.

PE fibres have a negative TCE in the axial direction. Polymeric matrices such as epoxy resin have a positive TCE, usually about $7 \times 10^{-5}\,°C^{-1}$. Kevlar and high-modulus PE fibres also have low compressive failure strain, only about 0.2%, and so the matrix curing shrinkage and the mismatch of TCE will cause the compressive failure of the fibres. They fail by forming kink bands along the fibres [2, 3]. The kink bands cause local stress concentrations and are potential sites for crack initiation. They are thus detrimental to the compression and fatigue strength of the composites. These stress concentrations also cause interfacial debonding, reducing the IFSS. In composite laminates, the residual stress can cause ply failure in absence of applied load [4].

The residual stress may be reduced by curing at a low temperature, but curing at high temperatures may be required to obtain the best matrix mechanical properties. The curing shrinkage and thermal residual stress may be reduced by optimizing the epoxy and curing agent and curing at different temperature stages [13]. The stress concentration at a kink band may be reduced by incorporation of a flexible thin layer at the interface [14]. In real composites, there exists a residual stress-free curing temperature because the fibre has a positive TCE while the matrix has a negative one [15]. This curing temperature can also be tailored by incorporating an appropriate inter-phase [16]. The overall residual stress can be reduced by adding an expanding monomer which expands in volume during polymerization to the epoxy [17]. These modifications were found to improve the composite compressive strength and interfacial shear strength.

On the other hand, curing shrinkage and mismatch of TCE usually produce a normal compressive residual stress at interface, which helps in obtaining good interfacial bonding. For example, carbon fibres have a radial TCE of $1.7 \times 10^{-5}\,°C^{-1}$ [5], which is much lower than that of epoxy matrices. A normal clamping stress on the fibre develops on cooling the matrix from the curing temperature. This clamping effect will improve the IFSS. Polymer fibres have a higher radial TCE than graphite fibres (Table I). The radial TCE of Kevlar fibres is $6.6 \times 10^{-5}\,°C^{-1}$ [16], which is very close to that of the epoxy matrix. The normal residual stress is close to null. Penn *et al.* [18] suggest that the lower interfacial clamping stress is the limiting factor causing the lower IFSS of Kevlar fibres.

The high-modulus PE fibres have an extraordinarily large positive radial TCE. It is approximately $13 \times 10^{-5}\,°C^{-1}$, according to the measurement of unit crystal dimensions as a function of temperature by Murthy *et al.* [7]. The TCE is much larger than that of commonly used epoxy resins ($7 \times 10^{-5}\,°C^{-1}$). The high radial TCE of the fibre will induce a normal tensile stress rather than normal compressive stress at the interface on cooling from a high curing temperature. Clearly, this normal tensile stress at the interface will significantly weaken the interface. In Part I of this paper [10] we have shown that the maximum IFSS for an ammonia plasma-treated PE fibre is 28 MPa while its apparent IFSS (as measured in a simple pull-out test) is 14 MPa. These values of $\tau_s$ and $\tau_a$ are three times lower than those for graphite fibre composites (Table I).

The plasma treatment used for these PE fibres is described by Li and Netravali [19]. The fibre surface is totally altered through the plasma deposition of an allylamine plasma polymer. The IFSS is improved by more than three times but is still considerably lower than that for other fibres. Others have also treated the fibres with various plasmas and acid etching [20–23]. All treatments give a weaker interface than that of Kevlar fibres.

An important experimental technique used to investigate the local fibre stress is micro-Raman spectroscopy. The principle here is that the frequencies of molecular vibrational modes change as bond lengths and bond angles change. Raman spectral peaks then shift as the molecular chains in the fibre are stretched or compressed. The shift has been found to be linear with local strain and stress up to quite high values of stress. Micro-Raman spectroscopy is particularly useful for measuring local fibre stress, because the laser light source used is easily focused on fibre surface to a spot less than 10 μm in diameter. The method has been demonstrated to follow the micromechanics of stress transfer in terms of stress or strain distribution along the fibre in model composites containing a poly(diacetylene) fibre [24, 25], a high-modulus PE fibre [10], or a Kevlar fibre [9]. It has also been used to measure the axial compressive residual stress in a single poly(diacetylene) single crystals [26, 27] and to determine the compressive failure strains of Kevlar and carbon fibres [11, 12] (see Table I).

In Part I of this paper [10] we used Raman Spectroscopy to measure the axial stress along a high-modulus PE fibre during fibre pull-out from an epoxy resin matrix. This allowed us to determine the maximum IFSS for that system. An approximate analysis for the micromechanics of stress transfer for composites, including the effects of friction and residual stress, was discussed. Boogh *et al.* [28] have studied the stress distribution in a high-modulus PE fibre embedded in epoxy and kept at a fixed strain. The efficiency of load transfer was determined for different surface treatments and epoxies in terms of a load transfer length. They showed that epoxy cured at a high temperature had a larger stress transfer length and lower IFSS. They did not demonstrate the existence of axial compressive stresses in their composites.

In this paper, we describe the use of Raman spectroscopy to measure the axial residual stresses after different curing conditions. We also show that Raman spectroscopy can be applied to measure the stress distribution $\sigma_f(x)$ along a fibre after interfacial debonding. According to Equation 39 of Part I [10]

$$\sigma_f(x) = \gamma (1 - e^{-\alpha(l_{eff}+x)}) \quad -l_{eff} \leqslant x \leqslant 0 \quad (1)$$

along a complete debonded interface, where $l_{eff}$ is the effective frictional transfer length. $\gamma$ and $\alpha$ are constants related to the interfacial normal stress $N_0$ and frictional coefficient $f$ as follows:

$$\gamma = \frac{N_0 E_f}{\nu_f}\left(\frac{1+\nu_m}{E_m} + \frac{1-\nu_f}{E_f}\right) \quad (2)$$

$$\alpha = 2fN_0/r_f\gamma \quad (3)$$

Where $E_f$ is the fibre Young's modulus, $E_m$ the matrix Young's modulus, $r_f$ the fibre radius, $\nu_f$ the Poisson's ratio of the fibre and $\nu_m$ the Poisson's ratio of the matrix. $\alpha$ and $\gamma$ can be obtained using a non-linear least-squares fitting procedure from the experimentally determined $\sigma_f(x)$. Then $N_0$ and $f$ can be calculated if $E_f$, $E_m$, $\nu_f$ and $\nu_m$ are known.

## 2. Experimental procedure

### 2.1. Materials and specimen preparation

The commercially available high-modulus PE fibres Spectra 900 were supplied by Allied Signal. DGEBA-type epoxy resin, DER 331, and tetraethylene pentamine curing agent, DEH 26, were obtained from Dow Chemical Company. They were mixed stoichiometrically according to the manufacturer's specifications. The curing conditions used were 4 h at 60 or 100 °C or at least overnight at room temperature. Some of these fibres were treated with an ammonia plasma for improved adhesion [29]. The single-fibre pull-out specimens were prepared using a silicone rubber mould technique described in detail in Part I of this paper [10, 19].

### 2.2. Raman spectroscopy

Raman spectra were obtained using a Spex 1877 triplemate spectrometer, equipped with an 1800 grooves/mm holographic grating at the spectrograph stage. The laser source was a 2 W $Ar^+$ laser (Coherent Nova 90-5) operating at 514.5 nm. A tunable excitation filter was used to reject spurious lines and background and a field stop was used to restrict the area of collection and reduce glare. The laser was focused on the specimen using a Leitz microscope with a 10× objective to a spot ~ 10 μm in diameter. The laser power reaching the specimen was about 25 mW. The scattered light was collected at 180° to the incident radiation with the same lens. The detection system was a diode array covering 400 $cm^{-1}$, an EG&G optical multi-channel analyzer and a PC. The spectra were calibrated using a neon or argon light source. The wave number shift of the peak of the C–C asymmetric stretch band is used to measure the tensile or compressive axial stress in the fibres. The measured value of the peak position of this band in free unstressed fibres taken at different times varied from 1063 to 1064.5 $cm^{-1}$. This is a significant variation, so the peak position of the free unstressed fibre was always measured and the peak shift relative to that value is quoted, not the absolute peak wavenumber.

### 2.3. Curing shrinkage and TCE of epoxy

The curing shrinkage of epoxy was measured according to the ASTM standard test method D2566-86 except for the dimensions of the moulded pieces. Instead of adopting the semi-circular mould, we used a rectangular mould 2 mm deep, 7 mm wide and 124 mm long. These cross-sectional dimensions are double those of the epoxy specimens used for Raman spectroscopy. A sample was moulded containing a thermocouple to check for heating during cure in these slightly larger specimens. No significant temperature rise was found during the exothermal curing reaction. These moulded specimens were subsequently used for the measurement of TCE following the procedures of ASTM standard test method D696-79.

### 2.4. Single-fibre pull-out test

Regular single-fibre pull-out tests were carried out on an Instron tensile machine model 1122. The load versus displacement was recorded on each test. The average IFSS, $\tau_a$, was calculated using

$$\tau_a = F_p/2\pi r_f l_e \quad (4)$$

where $l_e$ is the initial embedded fibre length and $F_p$ the peak pull-out load. If there were multiple peaks in the load–displacement curve, the first peak load was used for $F_p$. Ten specimens were tested for each condition.

For single-fibre pull-out tests using Raman spectroscopy the specimen was loaded using a dead weight. The epoxy was gripped in a small strain frame. The fibre ran horizontally and then passed over a smooth glass rod roller. The fibre end was gripped in a capstan clamp, which was then attached to a dead-weight hanger.

## 3. Results and discussion

### 3.1. Fibre compressive failure and kink bands

Fig. 1 contains optical photomicrographs of interfaces between fibre and epoxy for different curing conditions. Differences in the appearance of the interface are most obvious between an untreated fibre (Fig. 1d) and a treated fibre (Fig. 1f). In both specimens the epoxy was cured at 100 °C. The treated fibre is almost invisible, hardly distinguishable from the epoxy resin, whereas the interface between the untreated fibre and the epoxy shows as a strong dark line. This dark line is due to scattering of incident light by the interface. This indicates that a gap of the order of the wavelength of light (or more) exists between the fibre and epoxy. This dark line does not appear at the interface if the epoxy is cured at room temperature as can be seen in Fig. 1a.

Further optical observations of the interface were carried out using a hot stage. A specimen in which the

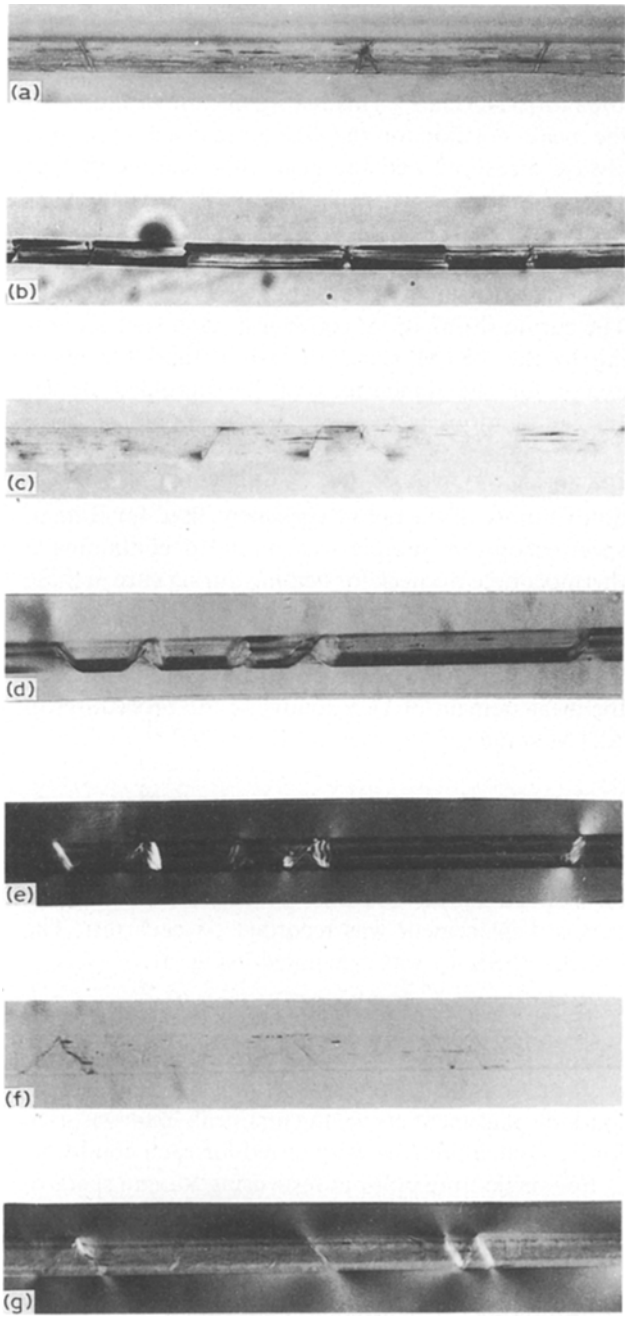


*Figure 1* Photomicrographs of Spectra fibre–epoxy interface: (a) untreated fibre in epoxy cured at room temperature, (b) untreated fibre in epoxy cured at room temperature and then post-heated to 100 °C, (c) untreated fibre in epoxy cured at 60 °C, (d) untreated fibre in epoxy cured at 100 °C, (e) as (d) with crossed polars at 0 and 90°, (f) treated fibre in epoxy cured at 100 °C, (g) as (f) with crossed polars at 0 and 90°.

epoxy had been cured at room temperature was heated to 100 °C and then cooled to room temperature. A dark line appeared at the interface during cooling, as shown in Fig. 1b, and it disappeared on heating the sample back up again to 100 °C. This confirms that the gap at the interface is caused by differential thermal contraction. A PE fibre has a larger radial TCE than the epoxy; the fibre shrinks more quickly in the radial direction than epoxy when the composite is cooled. For an untreated PE fibre, the interfacial bond strength is low, and the fibre separates from the epoxy, forming the gap at the interface.

The fibre radial TCE is $13 \times 10^{-5}\,°C^{-1}$ and the TCE of epoxy is $7 \times 10^{-5}\,°C^{-1}$ so that for a curing

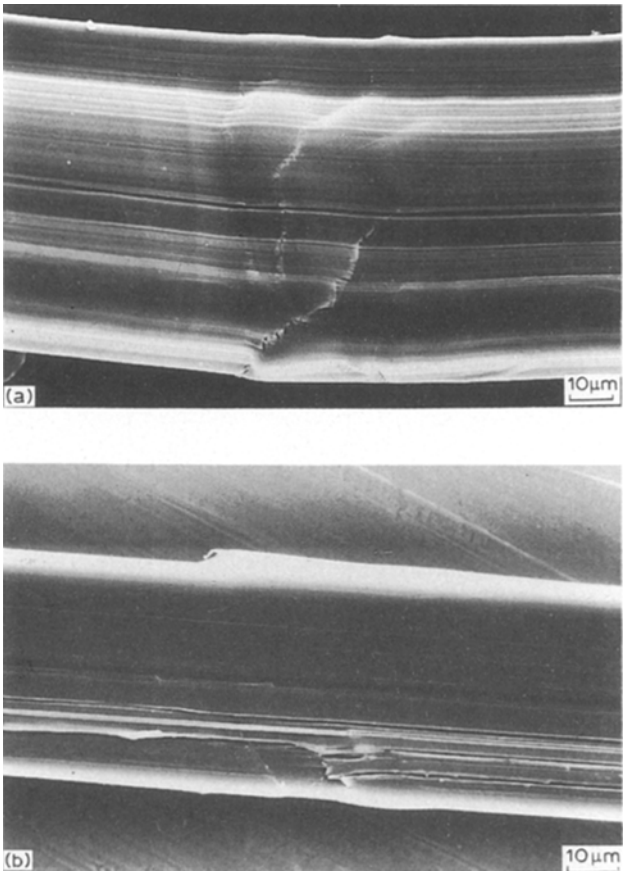


*Figure 2* SEM micrograph of (a) a kink band and (b) fibre surface irregularity.

temperature of 100 °C, the mismatch of TCE causes 0.5% normal residual strain of the fibre. 0.5% of 40 μm is 0.2 μm, about half a wavelength of the incident light, so a gap of this size will develop once the fibre is debonded from the epoxy. For treated fibres no dark line can be observed on cooling from 100 °C, so the improved bonding strength must prevent the separation of the fibre from epoxy. When interfacial debonding takes place during fibre pull out, a dark line is seen for all fibres.

The photomicrographs in Fig. 1 show that there are many kink bands along the fibres. Some of these kink bands exist before the composite is made. They are created during manufacturing or handling of the fibre; single fibres are quite delicate. Others are produced by the axial compressive stress resulting from the curing of the epoxy. Most of the kink bands show a plane at about 45° to the fibre axis, which indicates that they are caused by shear stress failure of the fibre. In Fig. 1 the kink bands appear as an oblique line or as an ellipse where the plane of the band intersects the fibre surface. The obliquity is shown more directly in an SEM micrograph in Fig. 2a.

Fig. 1e and g show the birefringence patterns around the embedded fibre, using crossed polars in the optical microscope. It can be seen that shear stress concentration exists in the epoxy near the kink bands. This shear stress concentration is another factor causing the interfacial debonding.

When untreated fibres are cured in epoxy at 60 °C and then cooled to room temperature, dark fringes appear at the interface only adjacent to the kink

bands, (Fig. 1c). Normal tension at the interface is not large enough to cause interfacial debonding by itself after curing at this temperature, but stress concentrations at the kink bands cause interfacial debonding nearby. When the curing temperature is above 100 °C, debonding extends along all the fibre *except* at the kink bands (Fig. 1d). This shows that good interfacial contact is still maintained at the kink band when debonding has occurred at all other positions along the fibre. A bump or other surface irregularity is often seen at kink bands, and Fig. 2 shows an example for the fibres used here. These bumps interlock mechanically with the matrix. Measurement of axial stress by Raman spectroscopy shows that an axial compressive residual stress exists along the untreated fibre even after interfacial debonding (Fig. 3). It is the irregularities at kink bands that prevent the fibre from recovering the axial residual compressive strain even though the interface is debonded and there is no normal clamping stress.

Fig. 3 shows the relative peak position shift of the 1063 $cm^{-1}$ band from PE fibres embedded in epoxy and the corresponding epoxy curing shrinkage. Three different curing temperatures were used. When the epoxy is cured at room temperature, residual stress due to thermal contraction will be zero. The compressive stress is then entirely due to the curing shrinkage of the epoxy, which is 0.14%. The band shift between the fibre in this composite and a free fibre is $+ 0.9 \pm 0.3$ $cm^{-1}$, so the shift factor for this fibre in compression is approximately 6.4 $cm^{-1}\%^{-1}$. According to previous published results for crystals of poly(diacetylene) and Kevlar and carbon fibres [11, 12, 26], Raman peak positions shift linearly in compression up to the compressive failure strain of the sample. Raman shift factors in compression were found to be approximately equal to those in tension. The shift factor of this Raman peak for a free PE fibre in tension was found to be $-5 \pm 0.5$ $cm^{-1}$ $GPa^{-1}$ [30, 31] and 6–10 $cm^{-1}\%^{-1}$ for fibres of a modulus 100–200 GPa [32]. We will therefore use the same constant shift factor of 6.4 $cm^{-1}\%^{-1}$ or 5 $cm^{-1}$ $GPa^{-1}$ for fibres in tension and in compression when converting the peak shift to fibre axial strain or stress.

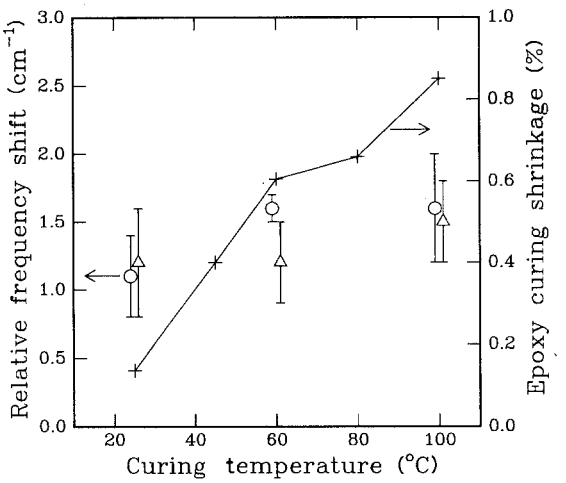


*Figure 3* Relative peak frequency shift of C–C asymmetric stretch bands and epoxy curing shrinkage at different curing temperatures for (△) treated and (○) untreated fibres in epoxy.

Further small shifts of peak position to higher wavenumbers for both treated and untreated fibres were found when the epoxy was cured at higher temperatures, as shown in Fig. 3. The difference is due to the mismatch of TCE which causes residual stress on cooling the composite to room temperature. The TCE of the epoxy resins, $\alpha_m$, cured at 100 °C is found to be $6.3 \times 10^{-5}$ $°C^{-1}$ below 85 °C, the glass transition temperature, and $7.3 \times 10^{-5}$ $°C^{-1}$ above it. The fibres have a negative TCE in the fibre direction, $\alpha_f$, of about $-5.1 \times 10^{-6}$ $°C^{-1}$. In the single-fibre epoxy specimen, the fibre volume fraction is close to zero, and so the thermal residual strain of the fibre is simply $(\alpha_m - \alpha_f)\,\Delta T$, where $\Delta T$ is the difference between the curing temperature and room temperature. Accordingly, curing at 100 °C produces a thermal residual compressive strain of approximately 0.5%. The total linear contraction on curing and cooling was measured to be 0.85%. This means that the linear shrinkage due to curing at 100 °C is 0.35%. Using the shift factor of 6.4 $cm^{-1}\%^{-1}$ obtained from the shrinkage of the epoxy cured at room temperature, a 0.85% shrinkage strain should produce a peak shift of about 5 $cm^{-1}$.

From Fig. 3, the largest increase in shift found between fibres cured in epoxy at room temperature and those cured at 100 °C is only 0.5 $cm^{-1}$. This indicates that there is no further elastic deformation of the fibres, i.e. the thermal residual stress has caused compressive failure. The fibre compressive strain at failure is estimated to be 0.23% from the total shift in wavenumber of 1.4 $cm^{-1}$. Using the shift factor or 5–6 $cm^{-1}$ $GPa^{-1}$, the compressive strength is 0.2–0.3 GPa.

There may be large residual stresses in both axial and radial directions and both may affect the position of the Raman peak. Using the shift of the peak to determine the axial residual stress is thus complicated by the radial normal stress exerted on the fibre. When the epoxy is cured at room temperature, the volumetric shrinkage of epoxy induces a radial compressive stress in addition to axial compressive stress. This radial stress will enhance the intramolecular interaction and will increase the vibrational frequency. Cottle *et al.* [33] have noted that the C≡C band vibrational frequency shifted to larger wavenumber when a hydrostatic compressive stress was applied to poly(diacetylene) single crystals. Grubb and Li [31] found that the C–C asymmetric stretch frequency shifted to larger wavenumber by 1 $cm^{-1}$ when the fibre was cooled in liquid nitrogen, and attributed this effect to the intermolecular interaction enhanced by the lateral contraction of the fibre in liquid nitrogen. When the epoxy is cured at higher temperatures a normal interfacial tensile stress develops, reversing the effect on the Raman band.

The error bars in Fig. 3 show that the peak position for each curing condition has a variation of 0.4 $cm^{-1}$. Repeated measurement does not reduce this, as it is mainly due to local variations in stress along the fibre. The localized plastic deformation and different normal stress at kink bands will cause stress concentra-

tions and thus local axial stress variation of the fibre. The peak shift was measured at a number of kink bands along a single fibre, and at fibre positions between the kink bands. Fig. 4 shows the results of this test for a surface-treated fibre in epoxy cured at room temperature. Of 19 pairs comparing kink band and fibre, ten show kink bands having higher frequencies than the fibre. Only one shows a kink band with a lower frequency, and in the others the differences are less than the error of measurement, which is $\pm 0.3\ cm^{-1}$. A higher wavenumber at kink bands may be due to a larger compressive strain at that point in either the axial or the radial direction. On average, the difference is only $0.2\ cm^{-1}$, compared to the variation between different kink bands of $0.5\ cm^{-1}$ and the variation along the fibre of $0.4\ cm^{-1}$. This indicates that the variation of strain along the fibre is more important than the local effects of kink bands.

## 3.2. Single-fibre pull-out tests

Table II shows the average IFFS, $\tau_a$, obtained using Equation 4 on fibres of embedded length 1 mm. Treated fibres give values approximately three times larger than those from untreated fibres. Comparing fibres with the same surface condition, curing at the higher temperature gives a lower IFSS. Kalantar and Drzal [1] found that the IFSS for Kevlar fibres is not affected by the curing temperature but that for carbon fibres increases with curing temperature. Considering the radial TCE for these fibres, we can see that the normal stress caused by cooling changes from tensile stress for polyethylene fibres to nearly null for Kevlar and to compressive stress for carbon fibres. We can conclude that the interfacial normal stress is the cause of the observed effects of curing temperature.

Fig. 5 illustrates the stress–displacement curve from a single-fibre pull-out test with an embedded length of 0.3 mm. The fibre was plasma-treated and the epoxy cured at room temperature. The fibre stress increases with displacement until interfacial debonding occurs, at which point the fibre slips and the stress drops instantaneously. After this interfacial friction resists motion, and the axial fibre stress is very small compared to the peak stress required for interfacial debonding. This stress–displacement behaviour is very common in fibre pull-out tests for short embedded lengths. The axial stress during pull-out against friction is not steady, as may be expected from a fibre of irregular cross-section.

Stress–displacement curves for high-modulus PE fibres with an embedded length of 10 mm are typically very different, as shown in Fig. 6. In all the plots, the first drop in stress represents the complete debonding of interface and the start of fibre pull-out against friction. Except for untreated fibres cured at room

TABLE II The average IFSS obtained at a fibre embedded length 1 mm

| Fibre | Curing temperature (°C) | $\tau_a$, (MPa) |
|---|---|---|
| Treated | 25 | 5.8 ($\pm$ 1.4) |
| | 100 | 5.0 ($\pm$ 1.3) |
| Untreated | 25 | 2.1 ($\pm$ 0.7) |
| | 100 | 1.3 ($\pm$ 0.3) |

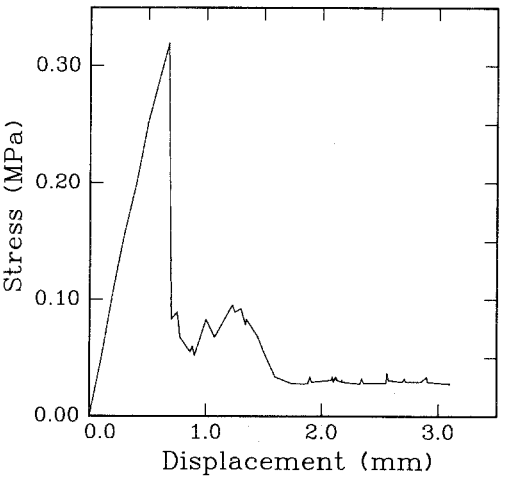


*Figure 5* Stress versus displacement for fibre pull-out from epoxy with an embedded length of 0.3 mm.

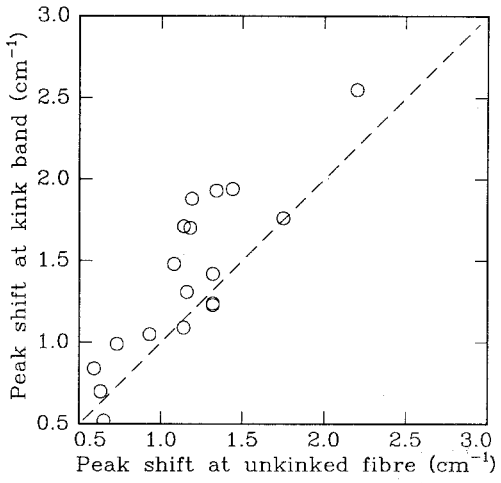


*Figure 4* Comparison of relative frequency shift of C–C asymmetric stretch bands of kink bands and fibre between kink bands. The location from which each data point is collected is randomly distributed along the fibre.

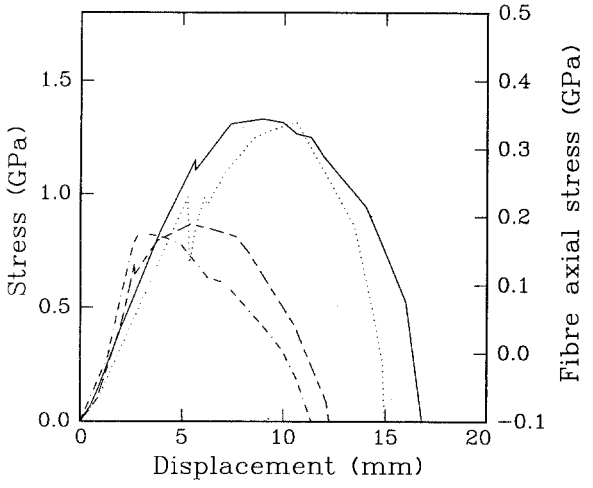


*Figure 6* Stress versus displacement for fibre pull-out from epoxy with an embedded length of 10 mm: effect of epoxy curing condition and fibre surface treatment. (——) Untreated, 25 °C; (– – –) untreated, 100 °C; (. . .) treated, 25 °C; (— · —) treated, 100 °C.

temperature, the stress increases again while the fibre is being pulled out, then drops after a significant amount of displacement. The stress in the frictional region increases with the fibre pull-out rate and this undoubtedly contributes to the high fracture toughness of PE composites.

It is difficult to explain why the frictional stress should increase with displacement. If the frictional stress on unit length of the fibre is constant, the stress should fall linearly with displacement as the length of the fibre in the matrix falls. A better analysis includes the Poisson's ratio effect on the normal forces. Where the fibre is under tension its diameter will be reduced, so the normal clamping force and the frictional effects will be less. The result of this is that most of the frictional load is generated near the end of the fibre. As it is pulled out the frictional load drops slowly at first, and then more rapidly, but this analysis cannot predict a rise.

A more realistic view of the resistance to motion, especially in cases where the normal stress on the fibre is negative (tensile), is to concentrate on the resistance to the motion of kink bands (and any other irregularities in the fibre) which have a larger local diameter. As soon as they move out of their original location, where the matrix will have had a larger hole, there will be great resistance to motion. The fibre is then seen as an elastic string containing knots along its length, and the resistance to pull-out comes from the knots. The simplest view is to take the resistance to knot motion to be due to elastic or viscoelastic deformation of the matrix. The decrement of tensile force at each knot is then proportional to the displacement or the rate of displacement of that knot. The decrement of displacement is the elastic stretch of the fibre between adjacent knots, proportional to the local tensile stress. A recurrence relation results, giving a solution of exponentially falling pull-out stress with displacement. To obtain an increase in frictional stress it must be imagined that the knots have increasing difficulty in moving through the matrix. They could perhaps act as snow-ploughs, building up plastically deformed material that continues to impede their progress. The increase in frictional stress maximum with rate of deformation might be taken to indicate an effect of frictional heating. If the energy is dissipated locally, the fibre will heat up and increase in radius, increasing the normal force and the heat dissipated. Unfortunately the thermal diffusivity of the matrix and the known small amount of energy dissipated limits the temperature rise to a few degrees.

Comparing the pull-out of the untreated and treated fibres from epoxy cured under different conditions, the fibre surface treatments not only improve the IFSS but also increase the frictional stresses. The maximum frictional pull-out loads are $2.0 \pm 0.4$ and $1.9 \pm 0.4$ GPa for treated fibre with epoxy cured at room temperature and 100 °C, respectively, whereas they are only $0.9 \pm 0.2$ GPa for untreated fibres under either of these curing conditions. Previous microscopy [29] has shown that the ammonia plasma treatments do not cause any surface roughening. It therefore seems unlikely that the surface treatment will significantly affect the frictional coefficient. The increased frictional resistance is then due to the larger radial normal stress and better mechanical interlocking effect that builds up after interfacial bonding. It will be shown later that normal stress is much larger for the treated fibre than for untreated fibre.

For fibres with the same surface treatment, the maximum frictional loads do not depend on the curing temperature. This is because there are two competing effects in operation. At a higher curing temperature the axial compressive stress causes the formation of more kink bands, enhancing the frictional resistance. However, the radial misfit between the fibre and epoxy is reduced up to the temperature where matrix shrinkage and thermal contraction mismatch.

### 3.3. Stress transfer in plasma-treated and untreated fibres

Fig. 7 shows the 1063 $cm^{-1}$ Raman band shifts for a plasma-treated fibre loaded at 0.4 GPa using dead weights. This is well below the interfacial debonding stress of 1 GPa obtained from a regular single-fibre pull-out test (Fig. 6). Even at this stress, debonding occurred due to creep at the interface, and a dark line appeared along the fibre starting at its entrance into the epoxy. The debonded part of the interface is only 0.2 mm long but it contains the largest part of the frequency shift. The shear stress in this debonded interface is 17.8 MPa. At the end of this dark line, the debonding front where debonding is just taking place, the frequency shift is approximately $+1$ $cm^{-1}$. The fibre at this point is in compression with an axial compressive stress of 0.2 GPa. All the fibre still bonded to the matrix remains in compression, with little change in stress. These results are very different to those shown in Part I of this paper [10] for a treated Spectra 1000 fibre in epoxy cured at room temperature. There, the maximum IFSS was at the debonding front and so was the frequency shift. With the small tensile load applied in this case, the axial compressive stress in the bonded part is close to the

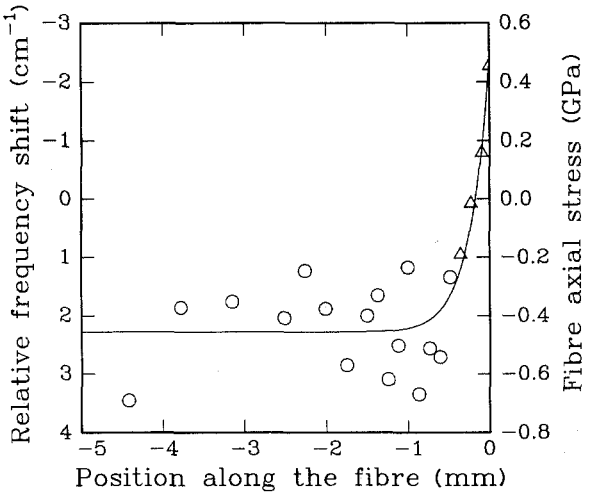


*Figure 7* Relative peak frequency shift of C–C asymmetric stretch bands and derived axial stress as a function of positions along the embedded fibre for a plasma-treated fibre at an external stress of 0.4 GPa: (○) bonded, (△) debonded.

compressive strength. Compressive failure of the fibre will restrict the range of elastic strain and thus the range of frequency shift.

How can the fibre debond from the matrix while it is still in axial compression? The debonding relates to a difference in matrix and fibre strain at the interface, which produces an interfacial shear stress. Here the matrix compression is large enough so that the interface fails while the fibre is still compressed. Numerically, following the analysis given in Part I [10], the stress at the debonding front $\sigma_d$ can be expressed as $\sigma_d = \sigma_r + 2\tau_s/\beta r_f \simeq \sigma_r + 0.36/r_f$, where $\sigma_r$ is the residual axial stress in the fibre, $\tau_s$ is the maximum IFSS and $r_f$ is the fibre radius. From Fig. 7 we can see that the average relative peak frequency shift is $2\,cm^{-1}$ in the bonded part of the fibre and so the fibre has an axial strain of $-0.3\%$ and an axial compressive residual stress of 0.4 GPa. Putting $\sigma_r = -0.4$ GPa and $r_f = 19\,\mu m$ in the above expression, $\sigma_d = -0.2$ GPa. This compressive stress agrees with the measurement described above.

The relative frequency shifts for an untreated fibre in epoxy cured at 100 °C are shown in Fig. 8. The shift and thus the axial stress changes slowly along the fibre. The initial slope is $0.46\,cm^{-1}\,mm^{-1}$, or $0.023\,GPa\,mm^{-1}$, so that the frictional interfacial shear stress is only 2.3 MPa. There is very little axial residual compressive stress, because the interface for the untreated fibre has already debonded. The residual fibre strain is gradually recovered as friction is established against the external stress. Fitting these data to Equation 1 (curve A in Fig. 8) gives values for $\alpha$ and $\gamma$. The best fit over the whole fibre produces a negative $\gamma$, which is physically meaningless. Taking the effective frictional stress transfer length $l_{eff}$ to be 5 mm, the region where the stress is clearly changing, and fitting Equation 1 in this region gives curve B in Fig. 8. This gives the values for $\alpha$ and $\gamma$ listed in Table III. The normal stress and frictional coefficient in the table are derived using Equations 2 and 3 and $E_f = 60$ GPa [29, 30], $E_m = 1.6$ GPa [34] and $\nu_m = \nu_f = 0.34$.

Fig. 9 shows the relative frequency shift along the fibre of a treated fibre during pull-out against friction at two external loads after the interface is fully debonded. The shift approaches zero at 6.0 and 9.0 mm at the lower and higher external stress, respectively, and these values were used as $l_{eff}$ in fitting to Equation 1. The two fits are shown as curves A and B. The results are summarized in Table III.

Comparing these frictional parameters $N_0$ and $f$ for the treated and untreated fibres, the maximum normal stress for the treated fibre is almost double that for the untreated fibre. The large variation in the frictional coefficient makes the difference between untreated and treated fibres not significant. This confirms that the maximum frictional stress is much higher for the treated fibres than for the untreated fibres, but intuition might lead one to expect that a different frictional coefficient would be the cause and not a different normal stress. How can plasma surface treatment result in a much larger interfacial normal stress? One possibility is through the chemistry of curing. The chemically active groups attached to the fibre surface by the plasma treatment could enhance cross-linking of epoxy at the interface. In that case the interfacial layer would have a higher modulus, and so the same mismatch in diameter between the fibre and epoxy

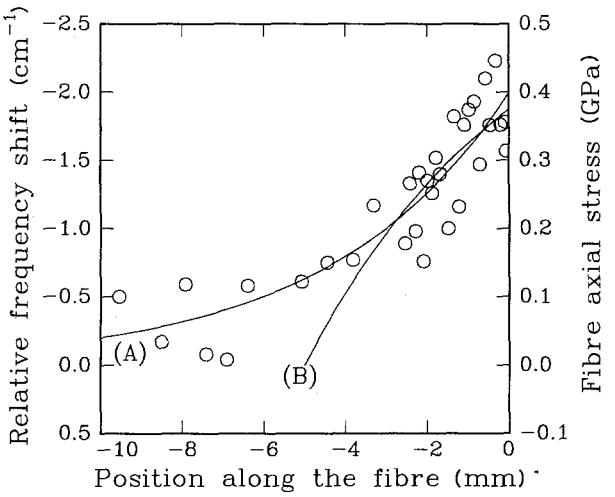


*Figure 8* (○) Relative peak frequency shift of C–C asymmetric stretch bands and derived axial stress at positions along the embedded fibre for an untreated fibre at an external stress of 0.4 GPa. For explanation of curves A and B see text.

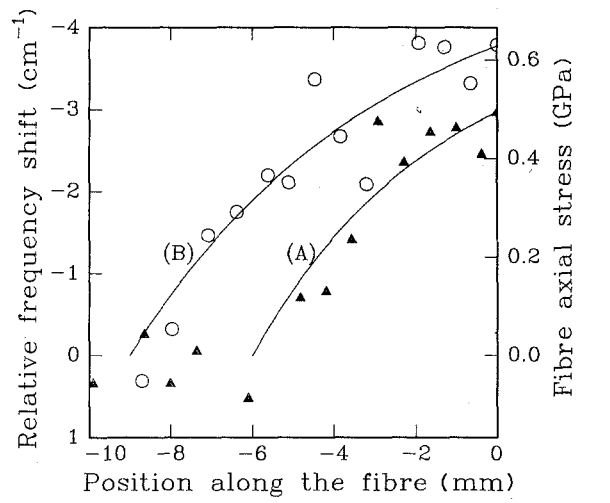


*Figure 9* Relative peak frequency shift of C–C asymmetric stretch bands and derived axial stress at positions along the embedded fibre for a treated fibre at external stresses of (○) 0.6 and (▲) 0.5 GPa after full interfacial debonding.

TABLE III Results of single-fibre pull-out over friction

| Fibre | $\alpha$ | $\gamma$ (GPa) | $N_0$ (MPa) | $f$ | $\sigma_m$ (GPa) |
|---|---|---|---|---|---|
| Untreated | $0.19 \pm 0.12$ | $0.38 \pm 0.1$ | $4.1 \pm 0.3$ | $0.26 \pm 0.17$ | $0.9 \pm 0.2$ |
| Treated | $0.1 \pm 0.064$ | $1.1 \pm 0.09$ | $7.2 \pm 0.6$ | $0.14 \pm 0.1$ | $2.0 \pm 0.4$ |

would produce a larger normal stress. It should be emphasized that this interfacial normal clamping stress during slippage after debonding does not arise from differential thermal shrinkage, but it comes from the misfit in diameter between fibre and epoxy after larger-diameter segments of the irregular fibre move out of their original locations.

## 4. Conclusions

The axial compressive residual stress in fibres due to volumetric curing shrinkage of the matrix due to the mismatch of TCE between fibre and curing matrix can be determined using Raman spectroscopy. The saturation of Raman peak shifting in compression indicates fibre compressive failure strain or stress. In the case of the high-modulus polyethylene fibres used here the compressive failure strain was 0.2–0.3%, and failure was by the formation of kink bands. The kink bands create local shear stress concentration and are sites for the initiation of interfacial debonding.

High-modulus polyethylene fibres have a larger radial TCE than epoxy resins, and at higher curing temperatures this causes a normal tensile stress at the fibre–epoxy interface on cooling to room temperature. Interfacial debonding occurs during cooling when the IFSS is low, in this case for untreated fibres. The radial TCE mismatch also causes the IFSS to decrease with increasing curing temperature. Plasma treatment of the fibre surface prevents interfacial debonding on cooling and so increases the IFSS dramatically. Nevertheless, the IFSS is still two to four times lower than that of other fibre composites and the large radial TCE of the polyethylene fibres is one reason for this.

Although the normal interfacial stress is initially tensile on cooling to room temperature, it changes to a compressive stress after interfacial debonding. Without a normal compressive stress there can be no friction. This normal stress comes from the irregularities in the fibre. Larger-diameter fibre segments will meet resistance to their motion as they move out of their original locations. Kink bands are one source of irregularities, but they may be removed, at least in part, by axial tension in the fibre.

The maximum pull-out stress in the frictional region is found to be much higher for plasma-treated fibres than for untreated fibres. The maximum normal stress is estimated from the axial stress distribution in the fibre by Raman spectroscopy. It is found that $N_0$ is $7.0 \pm 0.8$ MPa for a plasma-treated fibre and $4.1 \pm 0.3$ MPa for an untreated fibre, while the friction coefficients are $0.14 \pm 0.2$ and $0.26 \pm 0.17$, respectively. The fact that plasma treatment not only improves the IFSS but also causes a larger normal stress suggests that the fibre surface condition enhances the epoxy modulus in the interfacial region.

## Acknowledgements

This work is funded by the Cornell University Material Science Center which is supported by the National Science Foundation, DMR Grant No. 9121654. Mr J. Eun assisted with Raman spectroscopy and Mr E. Hsu worked on the single-fibre pull-out tests. The authors would like to express their appreciation to Professor A. Rouff and Y. Vohra for access to Raman spectroscope and to Professor P. Schwartz for reviewing the manuscript of this paper.

## References

1. J. KALANTAR and L. T. DRZAL, *J. Mater. Sci.* **25** (1990) 4186.
2. S. J. DETERESA and L. NICOLAIS, *Polym. Compos.* **9** (1988) 192.
3. L. T. DRZAL, "The Interfacial and Compressive Properties of Polybenzothiazole Fibers", AFWAL-TR-86-4003 (Air Force Wright Aeronautical Laboratories, Dayton, OH, 1986).
4. D. R. DONER and R. C. NOVAK, in Proceedings of 24th Annual Technical Conference, New York, Reinforced Plastics/Composites Division, Society of Plastics Industry, 1969, Paper 2-D.
5. J. A. NAIRN, *Polym. Compos.* **6** (1985) 123.
6. S. ROJSTACZER, D. COHN and G. MAROM, *J. Mater. Sci. Lett.* **4** (1985) 1233.
7. N. S. MURTHY, S. T. CORREALE and S. KAVESH, *Polym. Commun.* **31** (1990) 50.
8. B. MILLER, P. MURI and L. REBENFELD, *Compos. Technol.* **28** (1987) 17.
9. C. GALIOTIS, *ibid.* **42** (1991) 125.
10. Z. -F. LI and D. T. GRUBB, *J. Mater. Sci.*, in press.
11. H. JAHANKHANI and C. GALIOTIS, in "Interfaces in Polymer, Ceramic, and Metal Matrix Composites", edited by H. Ishida, (Elsevier Science, New York, 1988) p. 127.
12. N. MELANTIS, and C. GALIOTIS, *J. Mater. Sci.* **25** (1990) 5081.
13. V. B. GUPTA, L. T. DRZAL, C. Y.-C. LEE and M. J. RICH, *Polym. Eng. Sci.* **25** (1985) 812.
14. J. KARDOS, in "Molecular Characterization of Composite Interfaces", edited by H. Ishida and G. Kumar (Plenum, New York, 1985) p. 1.
15. H. T. HAHN, *J. Compos. Sci.* **10** (1976) 266.
16. J. A. NAIRN and P. ZOLLER, *J. Mater. Sci.* **20** (1985) 355.
17. P. W. K. LAM and M. R. PIGGOT, *ibid.* **24** (1989) 4068.
18. L. S. PENN, F. A. BYSTRY, W. KAPP and S. M. LEE, *Polym. Sci. Tech.* **27** (1985) 93.
19. Z. -F. LI and A. N. NETRAVALI, *J. Appl. Poylm. Sci.* **44** (1992) 333.
20. N. H. LADIZESKY, I. M. WARD and L. N. PHILLIPS, in Proceedings of ICCM-IV, "Progress in Science and Engineering of Composites", Tokyo, 1982, edited by T. Hayashi, K. Kawata and S. Umekawa, The Japanese Society for Composite Materials, p. 203.
21. A. R. POSTEMA, A. T. DOORNKAMP, J. G. MEIJER, H. vander VLEKKERT and A. J. PENNINGS, *Polym. Bull.* **16** (1986) 1.
22. N. X. NGUYEN, G. RIAHI, G. WOOD and A. PORSARTIP, in Proceedings of 33rd International SAMPE Symposium, Anaheim, California, 1988, p. 1721.
23. S. HOLMES and P. SCHWARTZ, *Compos. Sci. Technol.* **38** (1990) 1.
24. C. GALIOTIS, R. J. YOUNG, P. H. YEUNG and D. N. BATCHELDER, *J. Mater. Sci.* **19** (1984) 3640.
25. C. F. FAN, D. A. WALDMAN and S. L. HSU, *J. Polym. Sci. B: Polym. Phys.* **29** (1991) 235.
26. R. J. YOUNG, R. J. DAY, M. ZAKIKHANI and I. M. ROBINSON, *Compos. Sci. Technol.* **34** (1989) 243.
27. P. K. KIM, Y. Y. XU, C. CHANG and S. L. HSU, *J. Polymer* **27** (1986) 1547.
28. L. C. N. BOOGH, R. J. MEIER, H. H. KAUSCH and B. J. KIP, *J. Polym. Sci. B: Polym. Phys.* **30** (1992) 325.
29. Z.-F. LI, A. N. NETRAVALI and W. SACHSE, *J. Mater. Sci.* **26** (1992) 6631.
30. K. PRASAD and D. T. GRUBB, *J. Polym. Sci.* **B27** (1989) 381.

31. D. T. GRUBB and Z.-F. LI, *Polymer* **33** (1992) 2587.
32. B. J. KIP, M. C. P. van EIJK and E. J. MEIER, *J. Polym. Sci.* **B29** (1991) 99.
33. A. C. COTTLE, W. L. LEWIS and D. N. BATCHELDER, *J. Phys. C: Solid State Phys.* **11** (1978) 605.
34. A. N. NETRAVALI, R. B. HENSTENBURG, S. L. PHOENIX and P. SCHWARTZ, *Polym. Compos.* **10** (1989) 226.

*Received 10 April 1992*
*and accepted 4 January 1993*